

Phase response requirements between cross-coupled motion axes for handling qualities research simulators

William W. Chung

NASA, Ames Research Center, Moffett Field, CA

Ron Gerdes

NASA, Ames Research Center, Moffett Field, CA

Soren LaFirce

NASA, Ames Research Center, Moffett Field, CA

**AIAA Flight Simulation Technologies Conference, San Diego, CA, July 29-31, 1996,
Technical Papers (A96-35001 09-01), Reston, VA, American Institute of Aeronautics and
Astronautics, 1996**

An experiment was designed to study the effect of discrepancies between cross-coupled motion axes' responses, and to determine if phase response requirements for motion simulators are necessary for handling qualities research. Since the pilot is generally not located at the rotational center of a motion platform, this can produce distorted cues in a motion based flight simulator. The effect of phase response discrepancies between the roll and lateral cross-coupled motion axes was the focus of this experiment. A stability derivative model, which represents a fully decoupled aircraft response, was tailored to meet Level I rotorcraft handling qualities at low speed. The Vertical Motion Simulator, a gimballed motion system at NASA-Ames, provided the 6-DOF motion. Two low speed tasks, hover and side step, were used to evaluate the vehicle's handling qualities under three motion configurations and two visual delay configurations. The phase characteristics between the roll and lateral motion axes as well as the phase characteristics of the visual system were varied in the experiment. The test results indicated significant reduction in pilot workload and improved performance when the cross-coupled motion axes were in phase with each other and with the visual responses. (Author)

PHASE RESPONSE REQUIREMENTS BETWEEN CROSS-COUPLED MOTION AXES FOR HANDLING QUALITIES RESEARCH SIMULATORS

William W. Chung*, Ron Gerdes†, and Soren LaForce††
NASA Ames Research Center
Moffett Field, California

Abstract

An experiment was designed to study the effect of discrepancies between cross-coupled motion axes responses and to determine if phase response requirements for motion simulators is necessary for handling qualities research. Since the pilot is generally not located at the rotational center of a motion platform, this can produce distorted cues in a motion based flight simulator. For kinetically cross-coupled motion axes, such as roll and lateral, coordinated translational commands are required in order to compensate for induced linear accelerations caused by angular motion at the pilot station. The effect of phase response discrepancies between the roll and lateral cross-coupled motion axes was the focus of this experiment. A stability derivative model, which represents a fully decoupled aircraft response, was tailored to meet Level I rotorcraft handling qualities at low speed. The Vertical Motion Simulator, a gimbaled motion system at NASA Ames Research Center, provided the six degrees of freedom motion. The roll and lateral motion dynamics were modified to produce specific phase characteristics. This was required to study phase requirements between the roll angular acceleration and lateral specific force. Two low speed tasks, hover and side step, were used to evaluate the vehicle's handling qualities under three motion configurations and two visual delay configurations. The phase characteristics between the roll and lateral motion axes as well as the phase characteristics of the visual system were varied in the experiment. The test results indicated significant reduction in pilot workload and improved performance when the cross-coupled motion axes were in phase with each other and with the visual responses. A mismatch of phase response in the cross-coupled motion axes, up to 40 msec phase difference, led to increased pilot workload and poorer pilot handling qualities ratings in most instances. Due to a resulting large phase discrepancy

between the visual and motion cues, the results also suggest that visual delay compensation had little or no effect on pilots' handling qualities ratings under the given test conditions.

NOMENCLATURE

δ_c	pilot collective stick input, in.
δ_{lat}	pilot lateral stick input, in.
δ_{lon}	pilot longitudinal stick input, in.
δ_r	rudder pedal input, in.
ϕ	roll attitude, rad
$\varphi_{\omega f^2}$	mean-square-value over the specified frequency spectrum, n.d.
θ	pitch attitude, rad
τ	fitted time delay for visual and motion response, sec
ω_m	simulator angular rate vector, rad/sec,
$\dot{\omega}_m$	simulator angular acceleration vector, rad/sec ²
$\dot{\omega}_{pilot}$	helicopter angular acceleration vector, rad/sec ²
$\dot{\omega}_{m_cmd}$	simulator angular acceleration command vector, rad/sec ²
a_{mp}	linear accelerations generated by the motion simulator at the pilot station, ft/sec ²
a_{ps}	total linear accelerations sensed by the pilot, ft/sec ²
a_{pilot}	helicopter pilot station acceleration vector, ft/sec ²
a_{rc}	simulator rotational center (RC) acceleration vector, ft/sec ²
a_{rc_cmd}	simulator rotational center (RC) acceleration command vector, ft/sec ²
g	gravitational vector, ft/sec ²
$H(s)$	fitted linear transfer function of visual and motion response without the time delay
$L\delta_{lat}$	roll control power, rad/sec ² /in.
L_p	roll damping coefficient, 1/sec
$M\delta_{lon}$	pitch control power, rad/sec ² /in.
M_q	pitch damping coefficient, 1/sec
$N\delta_r$	yaw control power, rad/sec ² /in.
N_r	yaw damping coefficient, 1/sec
p	helicopter model roll rate, body axis, rad/sec
\dot{p}	helicopter roll angular acceleration, rad/sec ²

* Aerospace Engineer. Member of AIAA.

† Engineering Test Pilot. LOGICON SYSCON Services, Inc.

†† Simulation Engineer. LOGICON SYSCON Services, Inc.

Copyright © 1996 by the American Institute of Aeronautics and Astronautics, Inc. No copyright is asserted in the United States under Title 17, U.S. Code. The U.S. Government has a royalty-free license to exercise all rights under the copyright claimed herein for Governmental purposes. All other rights are reserved by the copyright owner.

$P(s)$	a linear representation of visual and motion response with time delay
\dot{p}_{cmd}	roll acceleration motion command, rad/sec^2
\dot{p}_m	roll motion acceleration response, rad/sec^2
q	helicopter model pitch rate, body axis, rad/sec
\dot{q}	helicopter pitch angular acceleration, rad/sec^2
\dot{q}_{cmd}	pitch acceleration motion command, rad/sec^2
\dot{q}_m	pitch motion acceleration response, rad/sec^2
r	helicopter model yaw rate, body axis, rad/sec
\dot{r}	helicopter yaw angular acceleration, rad/sec^2
\mathbf{r}	position vector of the pilot station with respect to simulator RC, ft
$\dot{\mathbf{r}}$	relative velocity vector of the pilot station with respect to simulator RC, ft/sec
$\ddot{\mathbf{r}}$	relative pilot station linear acceleration with respect to simulator RC, ft/sec^2
$T_a(s)$	transfer function of angular motion axis
T_m	direction cosine matrix from inertial to body axes of the simulator, n.d.
T_{mc}	direction cosine matrix from inertial to simulator body axes attitude excluding the component used for low frequency linear specific force, n.d.
$T_t(s)$	transfer function of translational motion axis
u	helicopter model translational velocity, x-body axis, ft/sec
v	helicopter model translational velocity, y-body axis, ft/sec
w	helicopter model translational velocity, z-body axis, ft/sec
$W_a(s)$	transfer function of angular washout filter
$W_t(s)$	transfer function of translational washout filter
x_ϵ	longitudinal position error for hover and sidestep tasks, ft
X_u	longitudinal damping coefficient, 1/sec
y_ϵ	lateral position error for hover task, ft
y_{cg}	lateral c.g. position for sidestep task, ft
Y_v	lateral damping coefficient, 1/sec
$Z\delta_c$	vertical control power, $ft/sec^2/in.$
Z_w	vertical damping coefficient, 1/sec

Introduction

Motion simulators are widely used in handling qualities research and flight training. These applications depend on onset accelerations produced by the motion platform in combination with cues presented to the pilot from visual displays, control force feel, audio effects, and instrumentation displays. The fidelity of the onset accelerations is subject to the modeled aircraft dynamic characteristics, motion system's dynamic characteristics, motion control algorithms, and displacement constraints. For ground based motion simulators, this presents quite a challenge, because the displacement constraints dominate the motion fidelity issue. Washout filters are generally used in motion control logic to generate initial onset accelerations

within the physical displacement constraints, i.e. the angular and translational limits. Therefore, the washout filters must be tuned to deliver consistent onset accelerations that complement the cues perceived by the pilot from other simulated devices.

To establish a direct correlation between simulation fidelity and handling qualities, Reference 1 suggests a criteria based on washout gains and phase characteristics as a measurement of motion cueing fidelity. Reference 2 follows the same frequency response approach and develops a 30 degree phase distortion criteria to compare perceived simulation cues for handling qualities evaluations. These were also the guidelines applied in developing the motion configurations for this experiment.

Reference 3 suggests that many motion cue errors are introduced in flight simulation due to physical constraints of motion platforms. Of all the motion cues perceived by the pilot, there is a fundamental element that is directly dependent on the kinetically cross-coupled motion system dynamic characteristics. This is a result of rigid body induced linear accelerations due to angular motion. Both Reference 4 and 5 indicate that translational accelerations sensed by the pilot are from the vestibular system and tactile mechanisms in the body. Due to the nature of human organ characteristics, lower frequency motion perception is sensed by the vestibular system and higher frequency motion perception is sensed by pressure from the pilot tactile mechanisms. Therefore, when the pilot station is not at the rotational center of the motion platform, an element of translational accelerations, i.e. induced linear accelerations, will be sensed by pilots due to angular motion. Induced linear accelerations are generally compensated in motion commands by assuming that the cross-coupled motion axis responses are the same. However, if the dynamic characteristics of two cross-coupled motion axes are not the same, or caused by different motion washout filter characteristics, discrepancies will be presented to the pilot and have an impact on the simulation fidelity. The objective of this experiment was to study the effect of phase differences between two kinetically cross-coupled motion axes and to determine if a requirement that defines acceptable phase discrepancy between the cross-coupled motion axes is necessary for ground based flight simulators.

Description of the Experiment

For a motion simulator where the pilot center of gravity is not at the rotational center of the motion platform, the specific force vector that is sensed by the pilot is governed by equation 1.

$$\mathbf{a}_{ps} = \mathbf{a}_{mp} - \mathbf{T}_m \cdot \mathbf{g} \quad (1)$$

The accelerations produced by the motion system at the pilot station, \mathbf{a}_{mp} , is defined by equation 2.

$$\mathbf{a}_{mp} = \mathbf{a}_{rc} + \dot{\mathbf{r}} + \boldsymbol{\omega}_m \times \mathbf{r} + \dot{\boldsymbol{\omega}}_m \times (\boldsymbol{\omega}_m \times \mathbf{r}) + 2 \boldsymbol{\omega}_m \times \dot{\mathbf{r}} \quad (2)$$

The position vector of the pilot, \mathbf{r} , is fixed relative to the rotational center, i.e. $\dot{\mathbf{r}}$ and $\ddot{\mathbf{r}}$ are zero. By assuming the rotational rate of the simulator cockpit, $\boldsymbol{\omega}_m$, is relatively small, equation 2 can be simplified to

$$\mathbf{a}_{mp} \approx \mathbf{a}_{rc} + \dot{\boldsymbol{\omega}}_m \times \mathbf{r} \quad (3)$$

The second term at the right hand side of equation 3 is the induced linear acceleration due to rotational motion, and the effect of this term is generally compensated in the motion commands such that this motion-platform-dependent term is not presented to the pilot. Similar reason also applies to the second term in equation 1 in compensating for the gravity component as a function of cab attitude. Therefore, the simulator translational and angular motion commands \mathbf{a}_{rc_cmd} and $\dot{\boldsymbol{\omega}}_{s_cmd}$ are defined as:

$$\mathbf{a}_{rc_cmd} = \mathbf{W}_t(s) \cdot \mathbf{a}_{pilot} - \mathbf{W}_a(s) \cdot \dot{\boldsymbol{\omega}}_{pilot} \times \mathbf{r} + \mathbf{W}_a(s) \cdot \mathbf{T}_{mc} \cdot \mathbf{g} \quad (4)$$

$$\dot{\boldsymbol{\omega}}_{m_cmd} = \mathbf{W}_a(s) \cdot \dot{\boldsymbol{\omega}}_{pilot} \quad (5)$$

But the actual simulator responses from translational and angular motion commands are determined by the individual motion axis dynamic characteristics, given by,

$$\mathbf{a}_{rc} = \mathbf{T}_t(s) \cdot \mathbf{a}_{rc_cmd} \quad (6)$$

$$\dot{\boldsymbol{\omega}}_m = \mathbf{T}_a(s) \cdot \dot{\boldsymbol{\omega}}_{m_cmd} \quad (7)$$

Therefore, the perceived motion cues in kinetically cross-coupled axes are dependent on the dynamic characteristics of both the washout filters and the motion hardware. If the overall dynamic characteristics, such as the phase characteristics of the lateral and roll motion responses, are not the same, then pilots will be subjected to erroneous linear acceleration cueing.

Math Model Description

A mathematical model in stability derivative form was developed to represent the dynamic characteristics of a rate command helicopter⁶ that is fully decoupled. The equations of motion are defined by equation 8 and 9.

$$\begin{bmatrix} \dot{u} \\ \dot{w} \\ \dot{q} \\ \dot{\theta} \end{bmatrix} = \begin{bmatrix} X_u & 0 & 0 & -g \\ 0 & Z_w & 0 & 0 \\ 0 & 0 & M_q & 0 \\ 0 & 0 & 1 & 0 \end{bmatrix} \begin{bmatrix} u \\ w \\ q \\ \theta \end{bmatrix} + \begin{bmatrix} 0 & 0 \\ Z_{\delta c} & 0 \\ 0 & M_{\delta e} \\ 0 & 0 \end{bmatrix} \begin{bmatrix} \delta_c \\ \delta_{lon} \end{bmatrix} \quad (8)$$

$$\begin{bmatrix} \dot{p} \\ \dot{r} \\ \dot{v} \\ \dot{\phi} \end{bmatrix} = \begin{bmatrix} L_p & 0 & 0 & 0 \\ 0 & N_r & 0 & 0 \\ 0 & 0 & Y_v & g \\ 1 & 0 & 0 & 0 \end{bmatrix} \begin{bmatrix} p \\ r \\ v \\ \phi \end{bmatrix} + \begin{bmatrix} L_{\delta_a} & 0 \\ 0 & N_{\delta_r} \\ 0 & 0 \\ 0 & 0 \end{bmatrix} \begin{bmatrix} \delta_{lat} \\ \delta_r \end{bmatrix} \quad (9)$$

Roll and pitch damping characteristics and control sensitivities are shown in Table 1. The aircraft characteristics were chosen to meet ADS-33D⁷ Rotorcraft Level I handling qualities performance in low speed.

Visual System

An interchangeable cab used on the Vertical Motion Simulator (VMS) is equipped with a visual system that uses an ESIG-3000 image generator by Evans & Sutherland. The cockpit field of view is shown in Fig. 1. The visual system has a pure transport delay of 60 msec from pilot's input to a full screen image update. With this visual time delay, the bandwidth on the roll response is reduced from 10 rad/sec to 4.5 rad/sec, which still meets the Level I handling qualities requirements. A compensation algorithm⁸ can be used to eliminate this visual delay, as was verified by Ref. 2. The visual time delay was one of the experimental parameters that was used to investigate the relationship between motion cross-coupled axes dynamic characteristics and visual delay characteristics.

Motion System

The VMS, as shown in Fig. 2, is a six degree-of-freedom motion platform that permits large excursions in the vertical and lateral axes. The vertical motion axis is driven by eight mechanically coupled 150-horsepower direct-current servomotors as outlined in Ref. 9. The lateral axis is driven by four 40-horsepower direct-current servomotors. Roll, pitch, yaw, and longitudinal are driven by four independent hydraulic systems with 2400 psi hydraulic pressure. The motion system's roll and lateral dynamic characteristics were tuned to three configurations for this experiment to study the effect of the phase difference between the two cross-coupled motion axes. The lateral accelerations due to yaw motion were not present due to the fact that the pilot longitudinal c.g. position was near to the gimbals rotational center for this experiment.

Three motion configurations were developed by using the visual system's 60 msec time delay as a reference. The VMS visual and motion system responses were fitted in a form defined by equation 10 which consists a linear transfer function, $H(s)$, and a time delay, τ .

$$P(s) = H(s) e^{-\tau s} \quad (10)$$

The characteristics of the visual system and the roll and lateral motion systems, $P(s)$, of the three motion configurations and their equivalent time delays are shown in Table 2. The equivalent time delay is defined as a pure time

delay that matches the phase response of $P(s)$ between .1 to 10 rad/sec. The frequency responses of these three motion configurations, i.e. acceleration output versus acceleration input, are shown in Fig. 3, 4, and 5. The first motion configuration, MC1, the matched visual and roll and lateral motion cueing, was developed such that both roll and lateral motion dynamic phase responses matched the visual phase response. The second motion configuration, MC2, delayed lateral motion, was developed to keep the roll axis phase response in phase with the visual system, but to delay the lateral axis phase response by 40 msec. The third motion configuration, MC3, delayed roll and lateral motion, was designed to keep the phase response of both roll and lateral motion axes 40 msec behind the visual response. The first configuration represents the best phase match of both visual response and roll-lateral motion response as perceived by the pilot. Dynamic response for each configuration was tuned to have a satisfactory phase response up to 10 rad/sec.

Motion Washout Filters

The VMS motion drive logic is shown in Fig. 6. Washout filters are applied to translational and rotational pilot station accelerations after being transferred to the inertial frame to keep the simulator within the physical travel limits. Turn coordination and induced acceleration compensation keep the cross-coupled motion commands in accordance to pilot position states relative to the rotational center. A low pass filter is used to tilt the cab in supplementing linear motion cueing at low frequency.

For the experiment, two motion washout configurations as shown in Fig. 7, were developed for the hover task to investigate the phase difference effect on pilots' handling qualities. The high fidelity configuration was developed to keep the phase of roll and lateral washout filters the same, i.e. $\phi(W_a(s)) = \phi(W_t(s))$, and to keep both angular and translational motion cueing within the high fidelity region according to Ref. 1. The mixed fidelity configuration represented a case investigated in Ref. 10.

For the sidestep task, the motion washout filters were configured as shown in Fig. 8. Again, the washout filter frequencies for roll and lateral axes were chosen to have the same phase characteristics.

The dynamic characteristics of the rotorcraft and perceived visual and motion cueing under each motion washout and motion dynamic configuration (with the visual time delay of 60 msec) are shown in Fig. 9 to 11. The acceptable fidelity range for the high fidelity washout configuration, based on the 30 degree phase distortion criteria from Ref. 2, is summarized in Table 3 for all three motion configurations. The acceptable fidelity range is defined as the frequency spectrum where the phase difference between perceived visual cueing and motion cueing is less than 30 degrees. The acceptable fidelity range for the same group of motion configurations but with a visual compensation of 60 msec are shown in the same table to present the effect of the

improved pilot perceived model response. As shown with the visual compensation, the pilot perceived an improved roll model response from a bandwidth of 4.5 rad/sec to 10 rad/sec as defined by the math model. However, phase improvement in the visual cueing alone would also increase the discrepancy between perceived visual and motion responses. As a result, a more restricted lateral-directional acceptable fidelity range over the frequency spectrum was developed.

Tasks

Two low speed tasks, Hover and Sidestep, were developed following the guidelines from ADS-33D under the no wind condition. Portions of the task procedures were modified to match the procedures developed in Ref. 2.

For the Hover task, the pilot was positioned at an angle with respect to the designated hover point, outlined in Fig. 12. The helicopter was initialized at 15 ft altitude. The pilot was asked to translate to a hover position over the desired hover point, with a ground speed of 6 kts, while maintaining the altitude. The desired hover point was defined by a hover target with a sight to indicate lateral position and height cues and a color-coded wall at a 45 degree angle to define longitudinal position cues. The transition to the hover point was to be achieved in one smooth maneuver, i.e. a smooth acceleration command followed by a smooth deceleration command. Creeping up to the final position was not allowed. The time for the pilot to stabilize at the desired hover point, from initiation of deceleration control input, was 15 seconds. Once in a stabilized hover, the pilot was asked to maintain hover position for 30 seconds. Rotorcraft deviations were measured from the desired hover point to determine pilots performance with respect to specified performance criteria, as given in Table 4.

For the Sidestep task, starting from a stabilized hover with the longitudinal axis of the rotorcraft oriented 90 degrees to the runway, as shown in Fig. 13, the pilot was asked to initiate a rapid and aggressive lateral translation, with a bank angle of at least 20 degrees, holding altitude constant with power. When the rotorcraft achieved a lateral velocity within 5 knots of the maximum allowable lateral airspeed, 30 knots, the pilot immediately initiated an aggressive deceleration to hover at constant altitude. The peak bank angle during deceleration was kept to at least 20 degrees, and occurred just before the rotorcraft came to a stop. Longitudinal and vertical position deviations were measured against the desired performance criteria, as shown in Table 4.

The visual data base was developed to provide visual cues for each task. Pylons and walls were color-coded such that the pilot could easily identify desirable and adequate performance envelopes. At the end of each task, the pilot was asked to give a handling qualities rating (HQR) based on the Cooper-Harper scale of Ref. 11.

A modified sidestep task was developed during the experiment to better reveal the significance of phase characteristics of the model-to-motion response. A closed loop task was added at the end of the sidestep maneuver by asking the pilot to hover before a designated pylon, with the same desirable performance criteria defined as before. Due to time limitations, only one pilot examined the modified sidestep task, and no pilot HQR was taken.

Results

The effects of kinetically cross-coupled motion dynamics were analyzed by studying HQRs and comments. Pilot control stick response and task performance data were also evaluated. The summary of the results are as follows:

Hover with high fidelity washout configuration

Pilot HQRs for three motion configurations are shown in Fig. 14. In comparing the first two motion configurations, i.e. matched cueing response (MC1) versus delayed lateral motion (MC2) two pilots, A and B, noted coordinated roll-lateral motion cueing which allowed them make accurate lateral inputs and pay more attention to longitudinal position control under the matched cueing configuration. Pilot B rated the matched cueing configuration better than the delayed lateral motion configuration. Pilot A felt that the matched cueing case (MC1) provided more solid motion cueing relative to the visual response, which reduced his physical and mental workload from that of the lagged lateral case. The increase in physical workload is strongly supported by the representative pilot lateral stick power spectral density (PSD) plot, given in Fig. 15, and the time trace of the pilot stick motion during the position-holding part of the task, Fig. 16. The power spectral density is the normalized energy distribution across the frequency spectrum. These data clearly showed that pilot workload associated with the lateral controller was reduced significantly across the frequency spectrum in the matched visual and motion cueing configuration. However, according to pilot A, the noted improvements in roll-lateral motion cueing response did not outweigh the required workload to hold the longitudinal position. Pilot C felt that both configurations required moderate pilot compensation to meet satisfactory performance criteria. He also felt that the delayed lateral motion had a slight advantage in pilot workload over the well matched case. For the delayed lateral motion configuration, jerkiness was among the common comments shared by all pilots.

The third motion configuration, motion lagged visual, was rated by two pilots, A and B. Pilot A rated this configuration worse than the matched cueing case and pilot B rated these two configurations with the same rating. Since the phase characteristics of the roll and lateral motion axes were the same in both configurations, the difference in pilot ratings could only result from the pilots' cueing preference, i.e. between the visual cueing and the motion cueing. Pilot A noted that some motion cues were lagging

while pilot B noted that visual and motion cues were in harmony.

A summary of pilot lateral control mean-square-value (ϕ^2) and pilot cutoff frequency (ω_c) from PSDs developed by using CIPHER, Ref. 12, is shown in Table 5. The pilot cutoff frequency approach is developed in Ref. 13 to compare pilot response characteristics under both flight and simulation conditions. By assuming a first order pilot response model, pilot cutoff frequency is defined as the frequency at half the power point of the total power spectral density of the given pilot control input, i.e. $\phi_c^2 / \phi_{\text{total}}^2 = 0.5$. The mean-square-value of the control with respect to the frequency spectra from 0 to ω_f , $\phi_{\omega_f}^2$, is equal to the total area under the PSD plot and is defined by equation 11,

$$\phi_{\omega_f}^2 = \frac{1}{2\pi} \int_0^{\omega_f} G_{\delta\delta} d\omega \quad (11)$$

where $G_{\delta\delta}$ contains the control power content as a function of frequency. Table 5 shows that under the matched cueing case, the total energy of the lateral control stick input consistently stays low among pilots in comparison with the other two mismatched conditions, which show comparable pilot cutoff frequencies.

Standard deviations of longitudinal and lateral position holding errors are given in Table 6. This table shows that pilots were able to maintain about the same level of performance regardless the test configurations, i.e. the change of motion parameters appeared to only affect the workload.

The longitudinal position cues were provided by the color-coded wall on the side window when in the stabilized hover position. Nonetheless, it did not provide an adequate range cueing sensitivity. This visual cueing deficiency combined with poorly coordinated pitch and surge dynamic characteristics with respect to visual cueing, Fig. 17, kept pilots' workload high in keeping longitudinal position within the satisfactory performance criteria, and made it more difficult in achieving Level I handling qualities performance.

Hover with mixed fidelity washout configuration

Pilot HQRs are shown in Fig. 14. The mixed fidelity motion configuration had a deviation in washout frequency between roll and lateral, 0.1 and 0.6 rad/sec respectively versus 0.3 for both axis in the high fidelity motion washout configuration. The washout gain on the lateral axis was also reduced from 0.9 to 0.4 in the mixed fidelity washout configuration. Roll washout gain was kept the same as the high fidelity washout case. The perceived roll and lateral motion cueing discrepancies as shown in Fig. 18 to 20, are much more significant at the low frequency range than in the high fidelity washout configuration. For pilot B and C,

who evaluated these tasks, both felt that the matched case had much better coordinated motion cueing than the other two cases. The pilot comments were very similar to those in the high fidelity motion configuration. The workload for the matched configuration again showed reduced lateral control energy by both pilots, as given in Fig. 21. A summary of pilot cutoff frequency is shown in Table 5. It is noted that from the PSD data, and pilot comments, that there is no significant difference between the high fidelity and mixed fidelity motion configurations. The large phase discrepancy between roll and lateral motion at low frequency did not have a significant effect on pilot workload, or on performance. The phase discrepancy effect in high frequency, however, had a definite effect on pilot workload.

Pilot B's HQR was consistent with the result from Ref. 10. Pilot A evaluated all three motion configurations in mixed fidelity configuration. However, his data was contaminated with an incorrect washout filter setup. Therefore, no conclusion can be drawn to confirm the consistency between the experiments.

Sidestep

Pilot HQRs for the sidestep task are shown in Fig. 22. There is no clear trend to indicate the effect of cross-coupled motion dynamic response. The results for this task were hampered by a lack of range cues when the pilot proceeded to a hover stop. The lack of longitudinal position information, lightly damped pitch motion characteristics, and visual-motion phase discrepancies again led to an appreciable amount of pilot effort in stabilizing the helicopter within desirable performance criteria.

For the modified closed-loop sidestep task, only one pilot data point was taken to evaluate two motion configurations, i.e. the matched cueing and delayed lateral motion cases, without taking any HQR. The time traces of the control stick and position error from deceleration to a stabilized hover are shown in Fig. 23. The power spectrum of the lateral stick is shown in Fig. 24. The power spectral density of lateral stick and the pilot cutoff frequency are shown in Table 5. The PSD did not show any significant differences between the two motion configurations. However, pilot A commented that overall control felt solid without any overshoot tendency in the matched cueing configuration. Desirable performance was easily achieved. With lagged lateral motion, however, it was harder to stabilize, and there was a tendency to overshoot. This is shown in the position error time trace, given in Fig. 23. The motion in the latter configuration "felt jerky and artificial". It also required at least moderate pilot compensation to achieve desired performance, which would be a Level 2 handling qualities rating.

Visual Delay

HQRs from pilot A and B with visual delay compensation turned on and off are shown in Fig. 25. From both pilots'

HQR on two washout configurations and three motion dynamic configurations, there is no significant difference in their ratings with and without the visual delay.

This result suggests that the improved model bandwidth response by removing the visual delay from the system was offset by the phase discrepancy between visual and motion cueing. Cueing discrepancies over the acceptable frequency range (Table 3) requires the pilot to mentally cross check the overall sensed model response, which meant increased pilot workload. The 30 degree phase distortion criteria provides a credible rationale for such a result.

Conclusions

A piloted motion based handling qualities flight simulation experiment was conducted to evaluate the significance of kinetically cross-coupled motion dynamic characteristics. Roll and lateral motion dynamic characteristics were perturbed for both precision hover and sidestep tasks. Visual delay and visual compensation were also evaluated under the same test conditions.

From pilot workload data, the phase characteristics of cross-coupled roll and lateral motion cueing has a significant effect on overall handling qualities of given tasks. Therefore, a requirement on cross-coupled motion axes phase characteristics with respect to visual response is strongly recommended to ensure the fidelity of flight simulation. The data from this experiment suggest that the roll dynamic response from motion cueing should at least match the visual response. The phase lag in lateral motion response with respect to the roll motion response should not be larger than 40 msec. Further investigations are required to define the specific phase criteria associated with the cross-coupled motion dynamic characteristics.

Visual delay compensation theoretically improves the simulation visual cueing responses, which should lead to better control bandwidth responses as well. Under the given test conditions, no noticeable pilot HQR or task performance improvement was found. That leads to the conclusion that the model response improvement made by visual cueing alone must be lost in the discrepancy between visual cueing and motion cueing. However, without the visual delay compensation, the vehicle's response characteristics is effectively reduced due to the inherited time delay in the digital flight simulation.

References

- 1 Sinacori, J. B.: The Determination of Some Requirements for a Helicopter Flight Research Simulation Facility. Contractor Report STI-TR-1097-1, September 1977.

²Mitchell, D. G.; and Hart, D. C.: Effects of Simulator Motion and Visual Characteristics on Rotorcraft Handling Qualities Evaluations. American Helicopter Society Conference on Piloting Vertical Flight Aircraft, Jan. 1993.

³Grant, P. R.; and Reid, Lloyd D: Motion Washout Filter Tuning: Rules and Requirements. AIAA Flight Simulation Technologies Conference, August 1995.

⁴Schroeder, J. A.; and Johnson, W. W.: Yaw Motion Cues in Helicopter Simulation. Proceedings of the AGARD Flight Vehicle Integration Panel Symposium on Flight Simulation, May 1995.

⁵Gum, D. R.: Modeling of the Human Force and Motion-Sensing Mechanisms. Air Force Human Resources Laboratory, AFHRL-TR-72-54, June 1973.

⁶Lewis, M. S.; Mansur, M. H.; Chen, R. T. N.: A Piloted Simulation of Helicopter Air Combat to Investigate Effects of Variations in Selected Performance and Control Response Characteristics. NASA TM-89438, 1987.

⁷Aeronautical Design Standard, Handling Qualities Requirements for Military Rotorcraft. ADS-33D, July 1994.

⁸McFarland, R. E.: Transport Delay Compensation for Computer-Generated Imagery Systems.. NASA TM 100084, Jan. 1988.

⁹Danek, G. L.: Vertical Motion Simulator Familiarization Guide. NASA TM-103923, May 1993.

¹⁰Hart, D. C.; and Mitchell, D. G.: A Simulation Investigation of Motion Cueing and Visual Time Delay Effects on Two Helicopter Tasks. NASA TM 110385, April 1996.

¹¹Cooper, G. E.; and Harper, R. P., Jr.: The Use of Pilot Rating in the Evaluation of Aircraft Handling Qualities. NASA TN D-5153, Apr. 1969.

¹²Tischler, M. B.; and Cauffman, M. G.: Frequency Response Method for Rotorcraft System Identification: Flight Applications to the BO-105 Coupled Rotor/Fuselage Dynamics. Journal of American Helicopter Society, Vol. 37, No. 3, pp. 3-17, July 1992.

Table 1. Damping characteristics and control sensitivity

X_u	Z_w	M_q	L_p	Y_v	N_r
(1/sec)	(1/sec)	(1/sec)	(1/sec)	(1/sec)	(1/sec)
0.0	-0.7	-4.3	-10.5	-0.12	-2.0
Z_{δ_c}	M_{δ_e}	L_{δ_a}	N_{δ_r}		
(ft/sec ² /in)	(rad/sec ² /in)	(rad/sec ² /in)	(rad/sec ² /in)		
-9.873	0.45	1.8	0.04		

Table 2. Fitted VMS visual and roll-lateral motion response model, and equivalent time delay

		Fitted model response, P(s)	Equivalent time delay, msec
Motion configuration	Visual	$e^{-0.060s}$	60
1. Well matched visual and motion	Roll	$\frac{77.9}{s+80} e^{-0.052s}$	65
	Lateral	$\frac{2.39(152.4)(s^2+12s+94)}{(s^2+21s+225)(s^2+16.2s+164.5)} e^{-0.01s}$	68
2. Delayed lateral motion	Roll	$\frac{77.9}{s+80} e^{-0.052s}$	65
	Lateral	$\frac{152.4}{s^2 + 16.2 s + 164.5} e^{-0.01s}$	108
3. Delayed roll-lateral motion	Roll	$\frac{19.75}{s+20} e^{-0.072s}$	107
	Lateral	$\frac{152.4}{s^2+16.2s+164.5} e^{-0.01s}$	108

Table 3. Acceptable simulation fidelity range for high fidelity washout filter configuration, rad/sec

Motion configuration	With visual delay				With visual compensation			
	Roll axis		Lateral axis		Roll axis		Lateral axis	
	Min	Max	Min	Max	Min	Max	Min	Max
1. matched visual and roll-lateral motion	0.8	>60	0.8	17	0.75	9	0.75	9
2. delayed lateral motion	0.8	>60	0.8	7.8	0.75	9	0.75	5
3. delayed roll and lateral motion	0.8	8.5	0.8	7.8	0.75	5	0.75	5

Table 4. Task performance criteria

Task	Position Tolerance (ft)		Altitude Tolerance (ft)		Heading Tolerance (deg)		Time to Complete (sec)	
	D	A	D	A	D	A	D	A
Hover	± 3	± 8	± 2	± 4	± 5	±10	< 15	< 30
Sidestep	± 20	± 50	± 10	± 15	± 10	± 15		

Table 5. Pilot lateral stick power spectrum density and pilot cut-off frequency for hover task

Pilot	Motion configuration	High fidelity washout		Mixed fidelity washout		Modified sidestep	
		$\phi_{\omega f^2}$	ω_c (rad/sec)	$\phi_{\omega f^2}$	ω_c (rad/sec)	$\phi_{\omega f^2}$	ω_c (rad/sec)
A	1. matched visual and roll-lateral motion	0.004	2.1			0.48	1.7
	2. delayed lateral motion	0.013	1.7			0.88	1.4
	3. delayed roll and lateral motion	0.015	2.4				
B	1. matched visual and roll-lateral motion	0.017	2.1	0.005	2.2		
	2. delayed lateral motion	0.055	2.4	0.059	2.1		
	3. delayed roll and lateral motion	0.065	1.8	0.037	1.9		
C	1. matched visual and roll-lateral motion	0.04	2.5	0.06	2.7		
	2. delayed lateral motion	0.051	2.4	0.037	3.3		
	3. delayed roll and lateral motion			0.055	4.1		

Table 6. Hover performance data with high fidelity washout configuration

Pilot	Motion configuration	Longitudinal position error (ft)				Lateral position error(ft)			
		Average	σ_{x_e}	Max	Min	Average	σ_{y_e}	Max	Min
A	1. matched visual and roll-lateral motion	-0.21	0.64	1.26	-1.08	0.1	0.44	1.27	-0.68
	2. delayed lateral motion	0.8	0.89	2.53	-1.12	0.24	0.41	1.26	-0.79
	3. delayed roll and lateral motion	0.9	0.88	2.53	-1.4	0.32	0.47	1.26	-0.80
B	1. matched visual and roll-lateral motion	0.03	1.34	2.04	-3.13	-0.04	0.71	1.0	-2.2
	2. delayed lateral motion	0.04	1.39	3.1	-2.42	-0.3	0.67	1.35	-1.32
	3. delayed roll and lateral motion	0.93	1.55	3.1	-3.1	0.81	0.67	2.4	-0.54
C	1. matched visual and roll-lateral motion	0.11	1.02	2.67	-1.72	-0.35	0.46	0.66	-1.57
	2. delayed lateral motion	0.17	0.98	1.26	-2.47	-0.03	0.57	1.15	-1.51
	3. delayed roll and lateral motion								

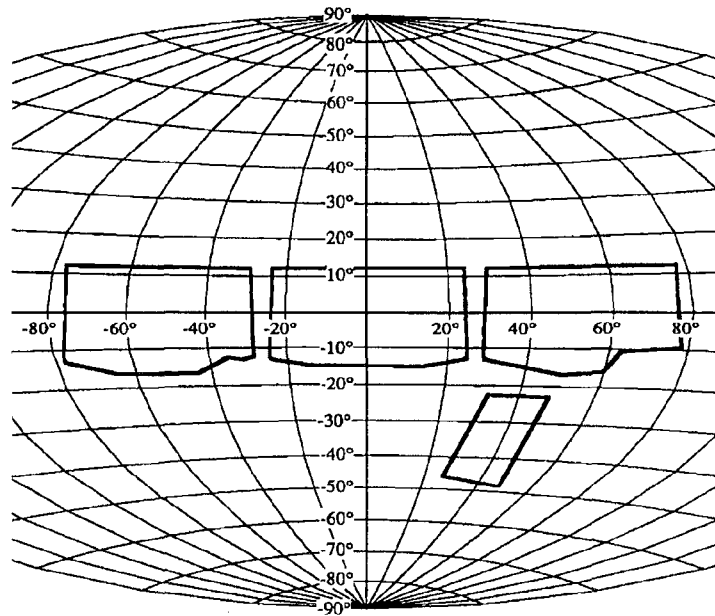


Figure 1. VMS R-cab display field of view

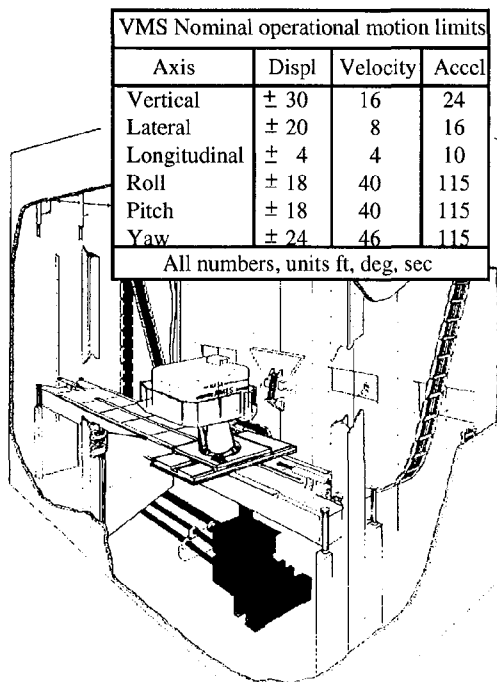


Figure 2. NASA Ames Research Center VMS Vertical Motion Simulator

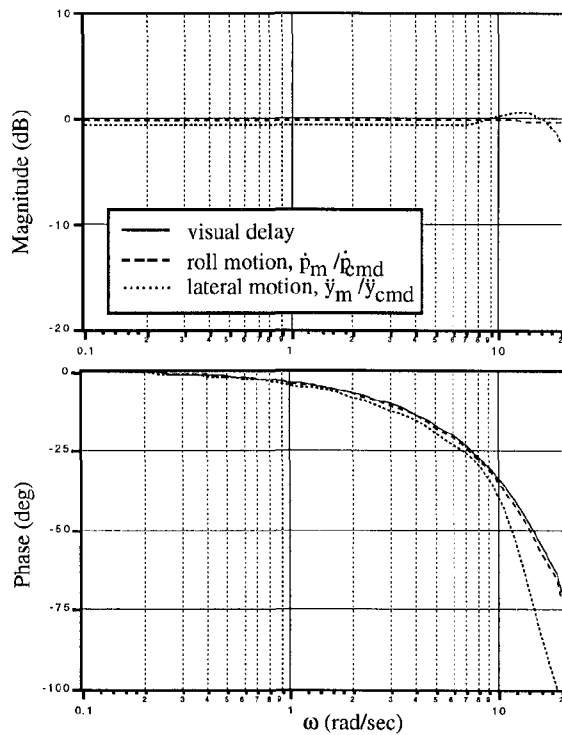


Figure 3. Matched visual, and roll and lateral motion configuration, MC1

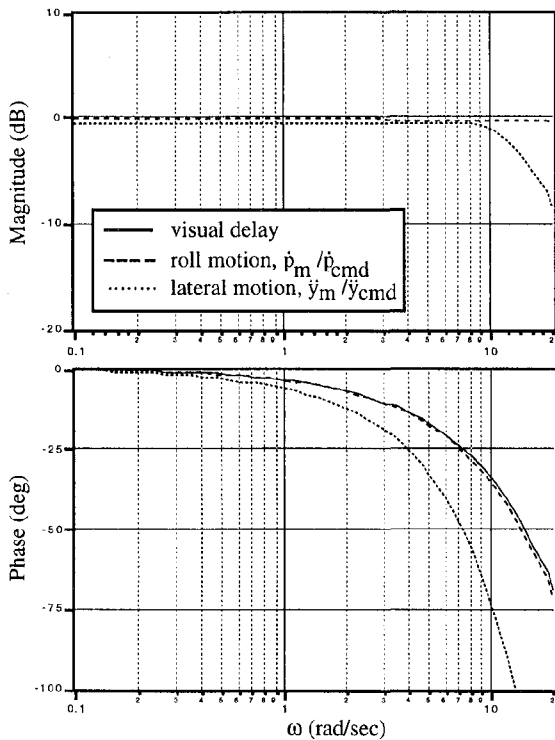


Figure 4. Delayed lateral motion configuration, MC2

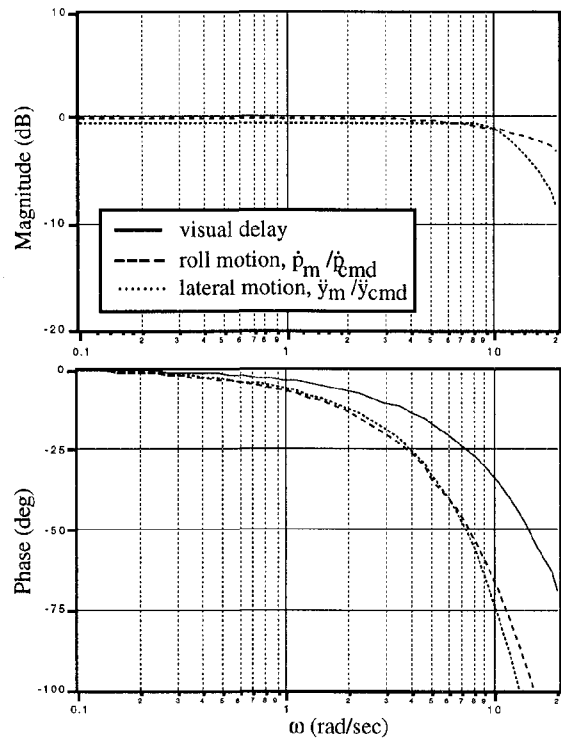


Figure 5. Delayed roll and lateral motion configuration, MC3

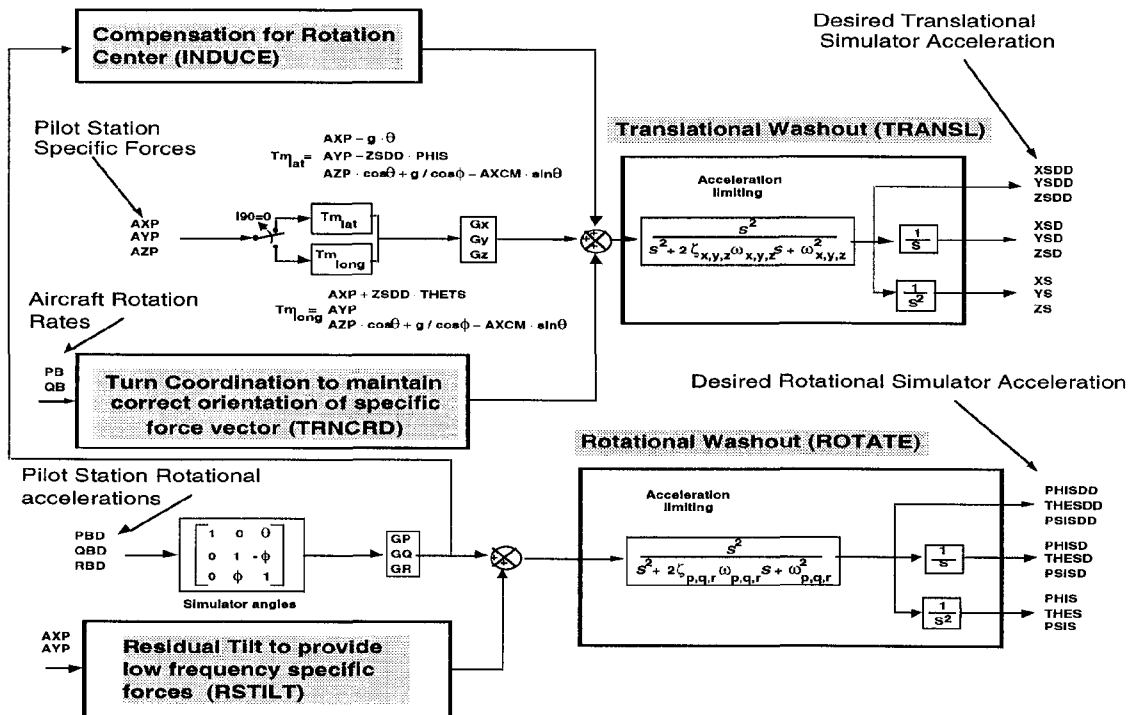


Figure 6. VMS motion drive commands block diagram

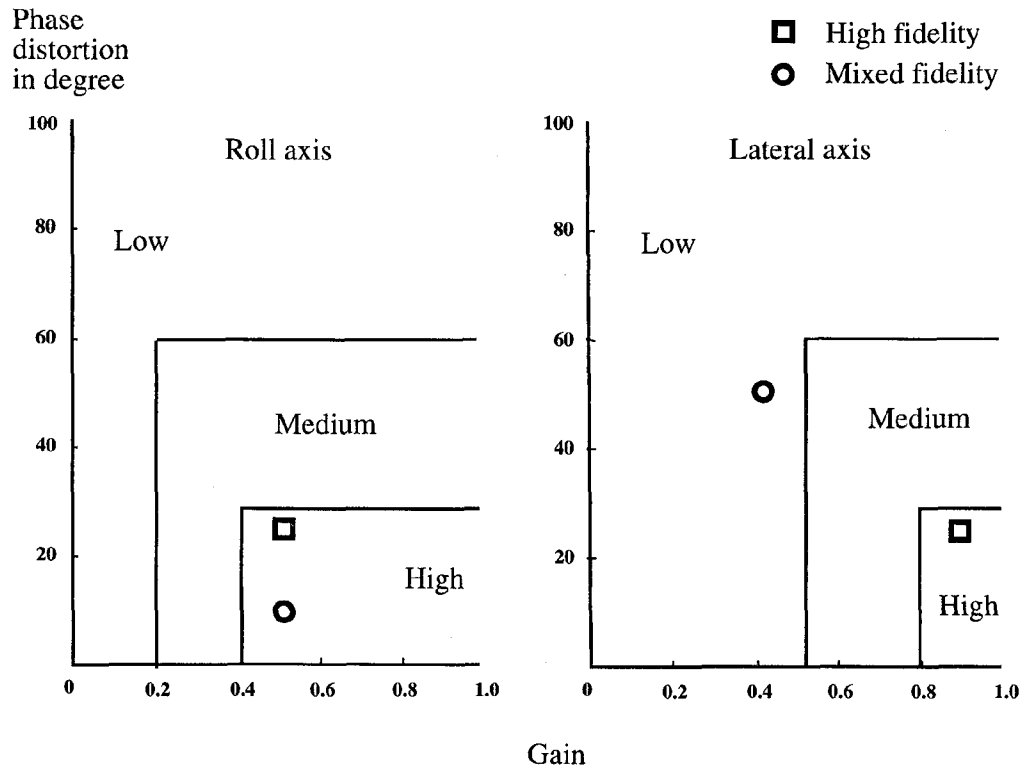


Figure 7. Motion cueing fidelity for hover task at 1 rad/sec

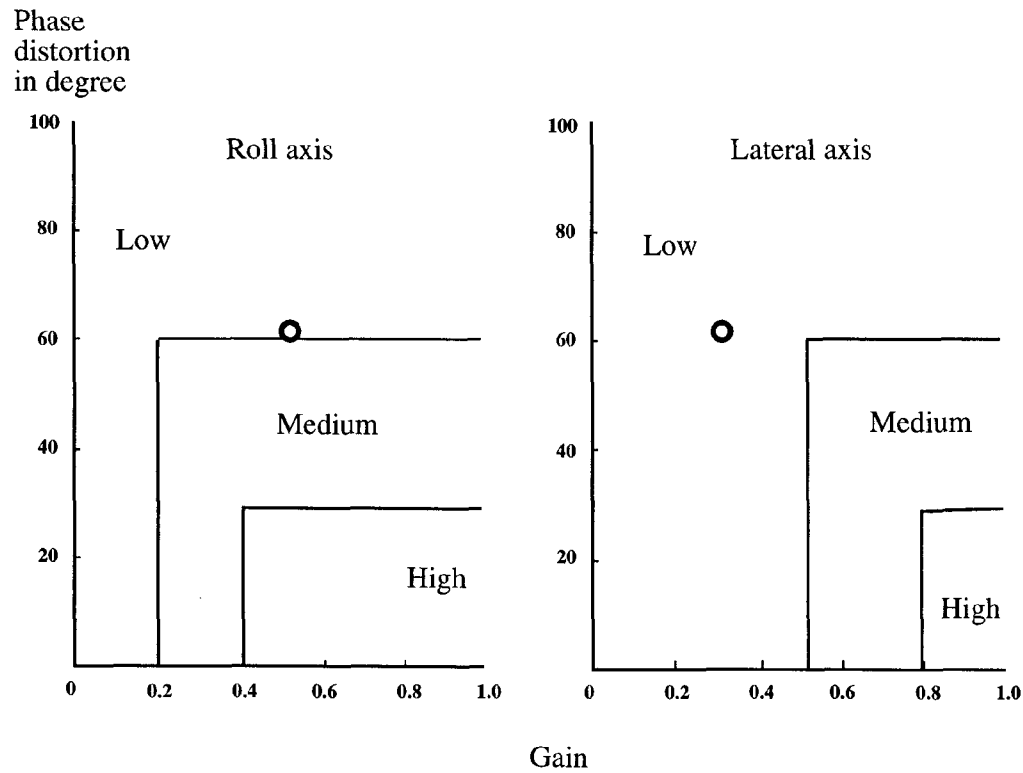


Figure 8. Motion cueing fidelity for sidestep task at 1 rad/sec

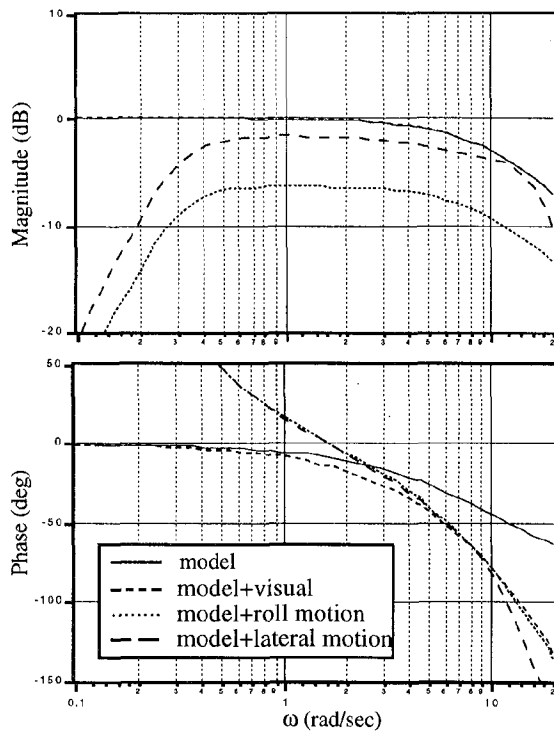


Figure 9. Roll model, and perceived visual and motion cueing responses in mathed cueing configuration, MC1

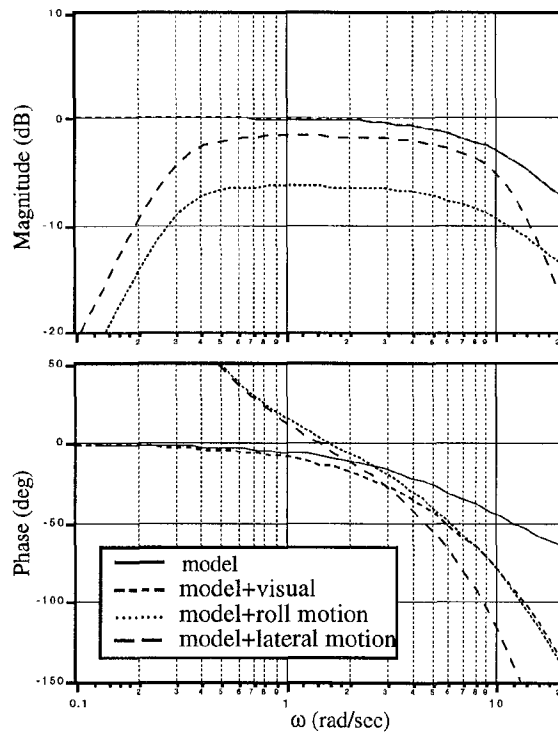


Figure 10. Roll model, and perceived visual and motion cueing responses in delayed lateral motion configuration, MC2

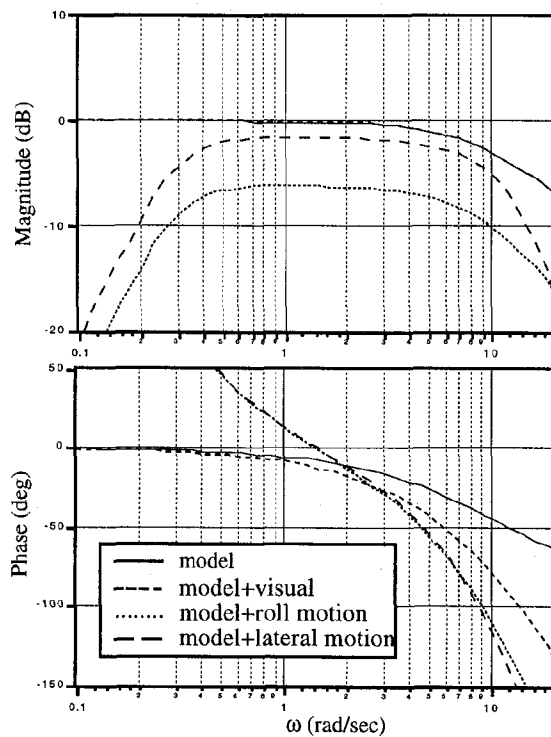


Figure 11. Roll model, and perceived visual and motion cueing responses in delayed motion configuration, MC3

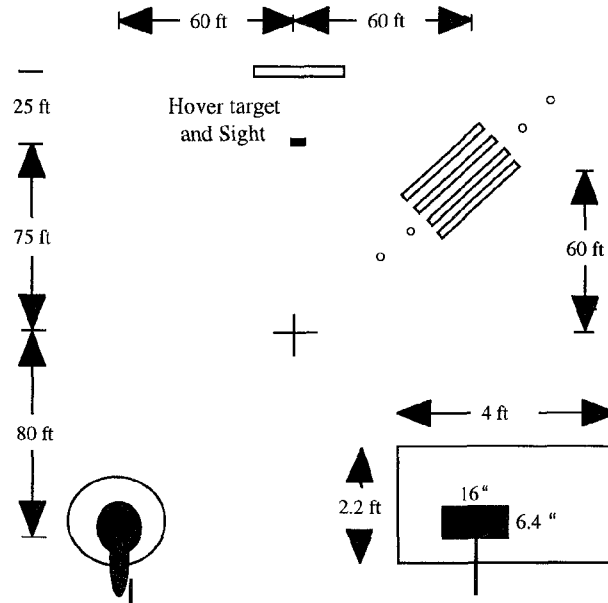


Figure 12. Hover task layout

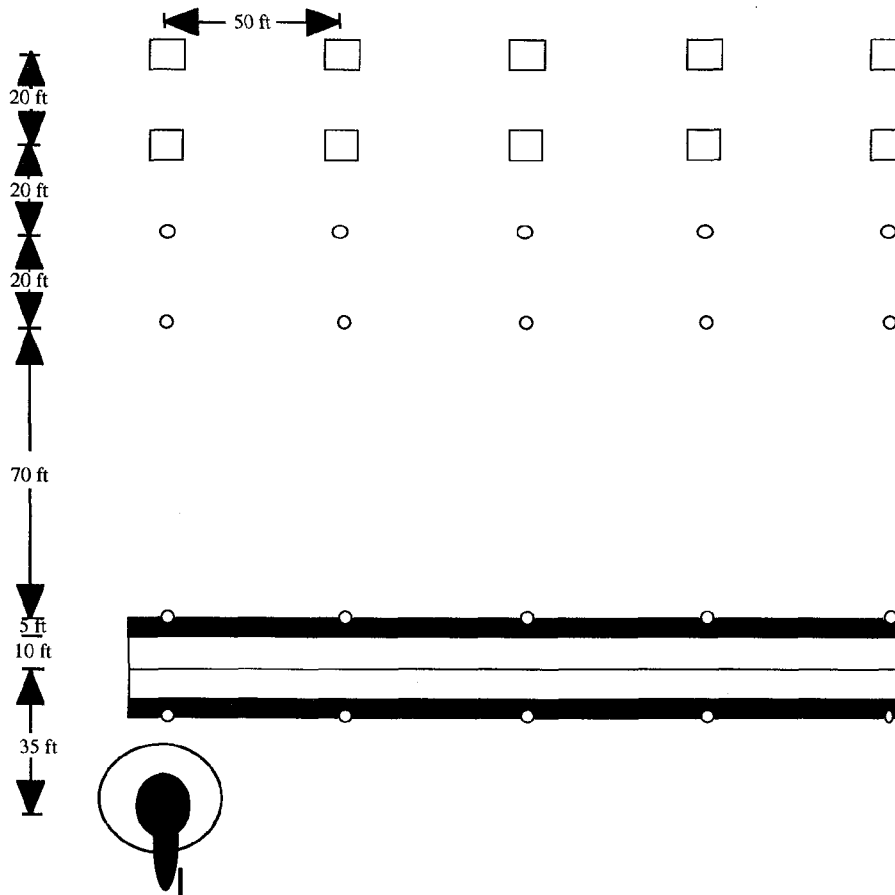


Figure 13. Sidestep task layout

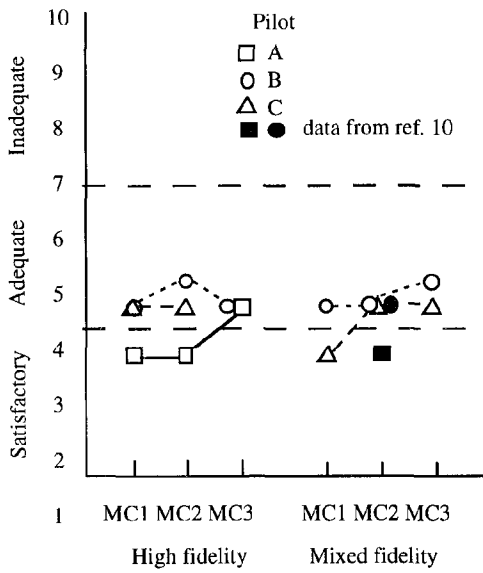


Figure 14. Pilot HQRs for hover task

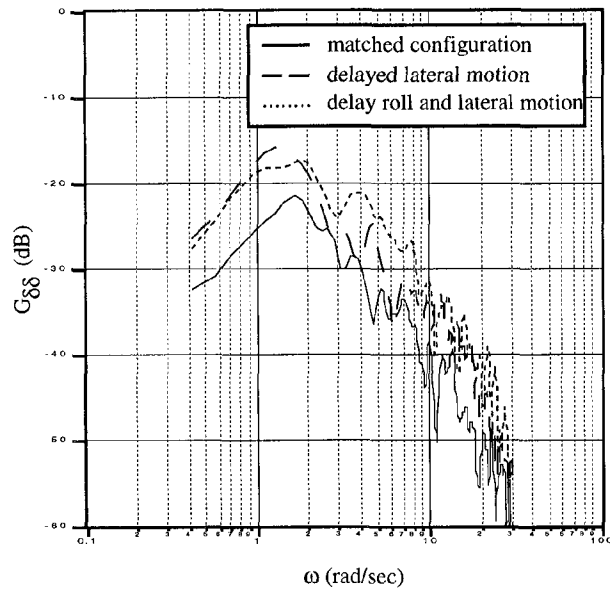


Figure 15. Pilot lateral control stick power spectral density response for hover with high fidelity motion cueing configuration

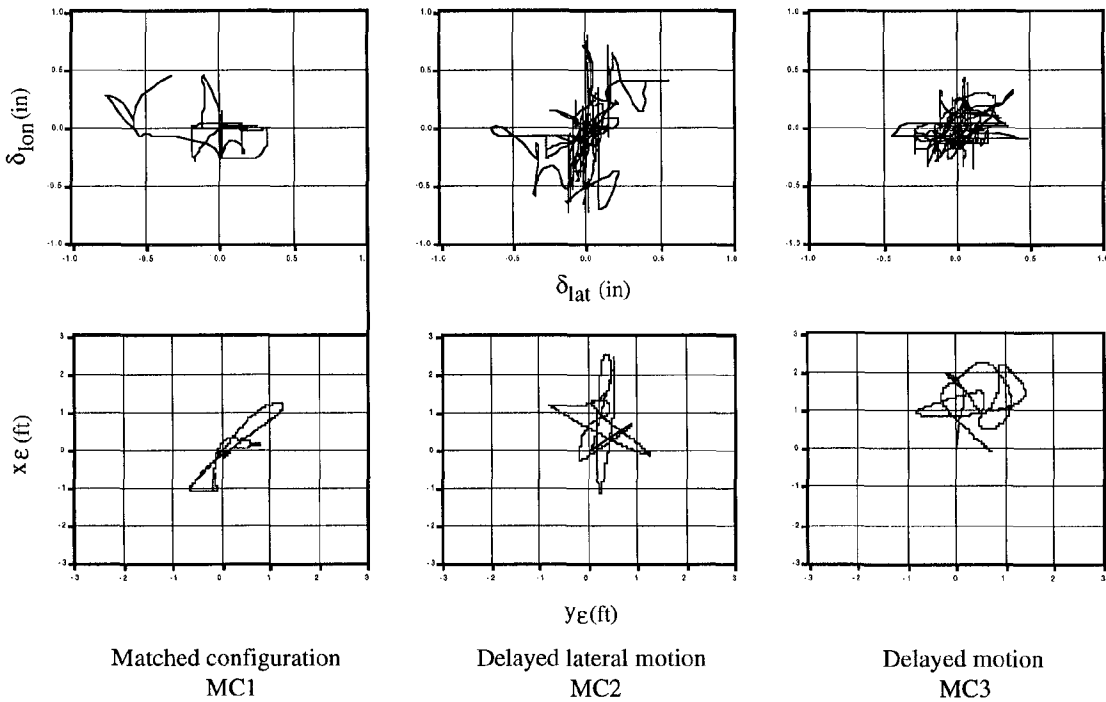


Figure 16. Pilot control stick and position error time traces for the hover task

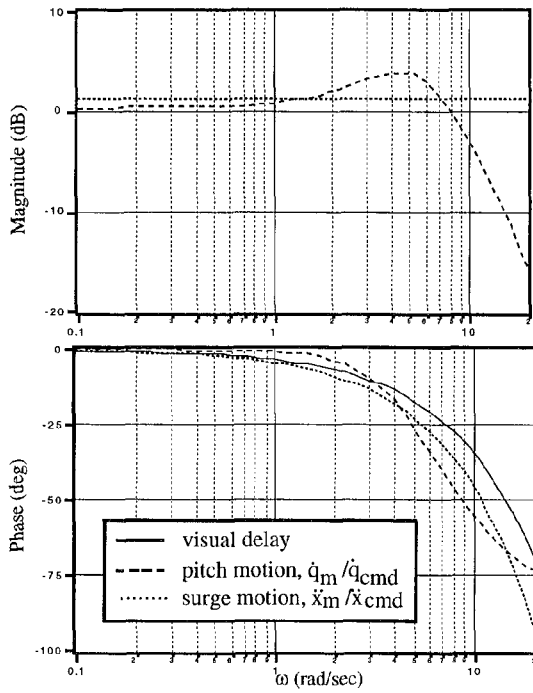


Figure 17. Visual delay, and pitch and surge response

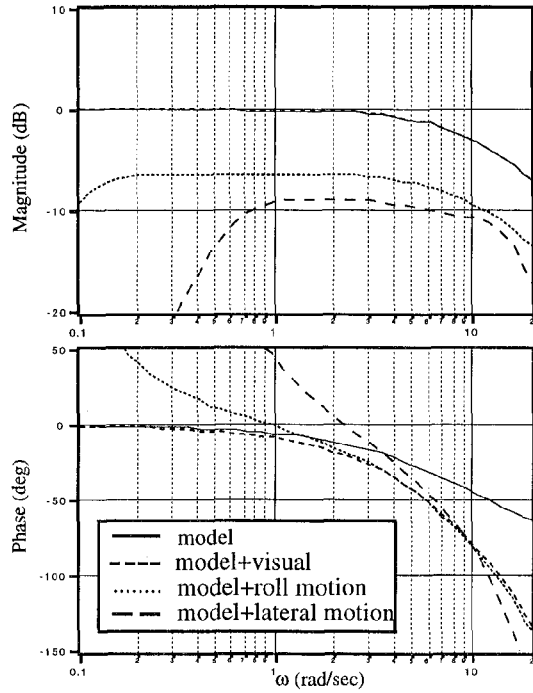


Figure 18. Roll model, and perceived visual and motion responses in matched, MC1, and mixed fidelity configuration

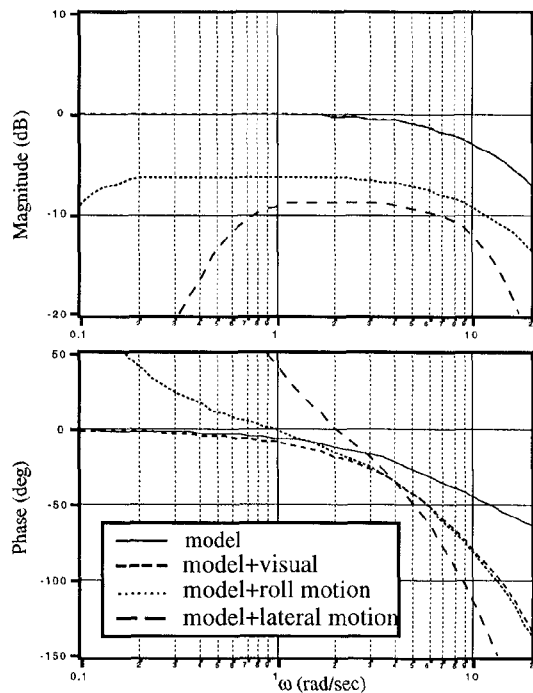


Figure 19. Roll model, and perceived visual and motion responses in delayed lateral motion, MC2, and mixed fidelity configuration

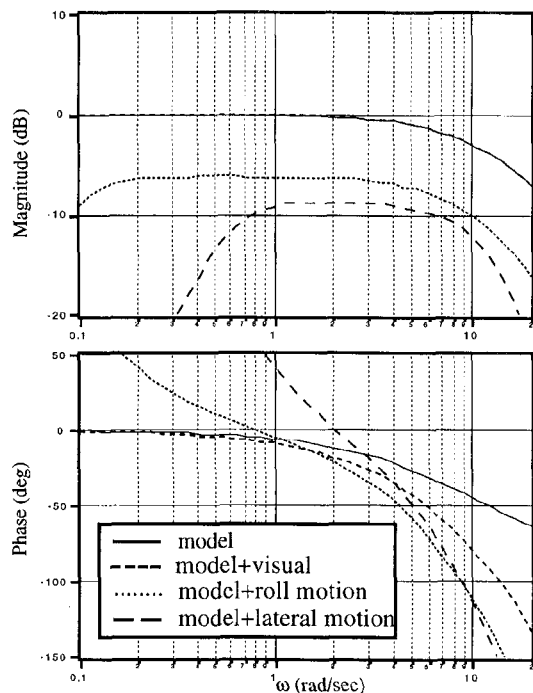


Figure 20. Roll model, and perceived visual and motion responses in delayed motion, MC3, and mixed fidelity configuration

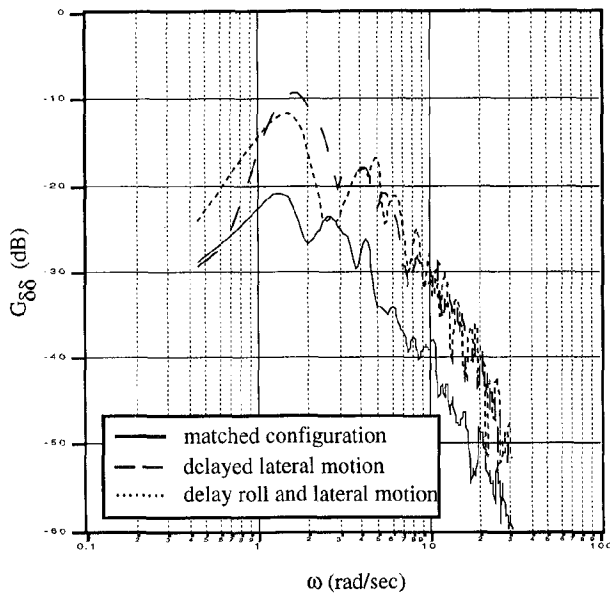


Figure 21. Pilot lateral control stick power spectral density response for hover with mixed fidelity motion cueing configuration

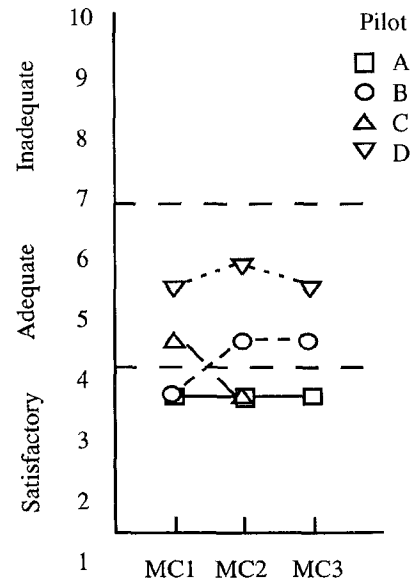


Figure 22. Pilots HQR for sidestep task with visual delay

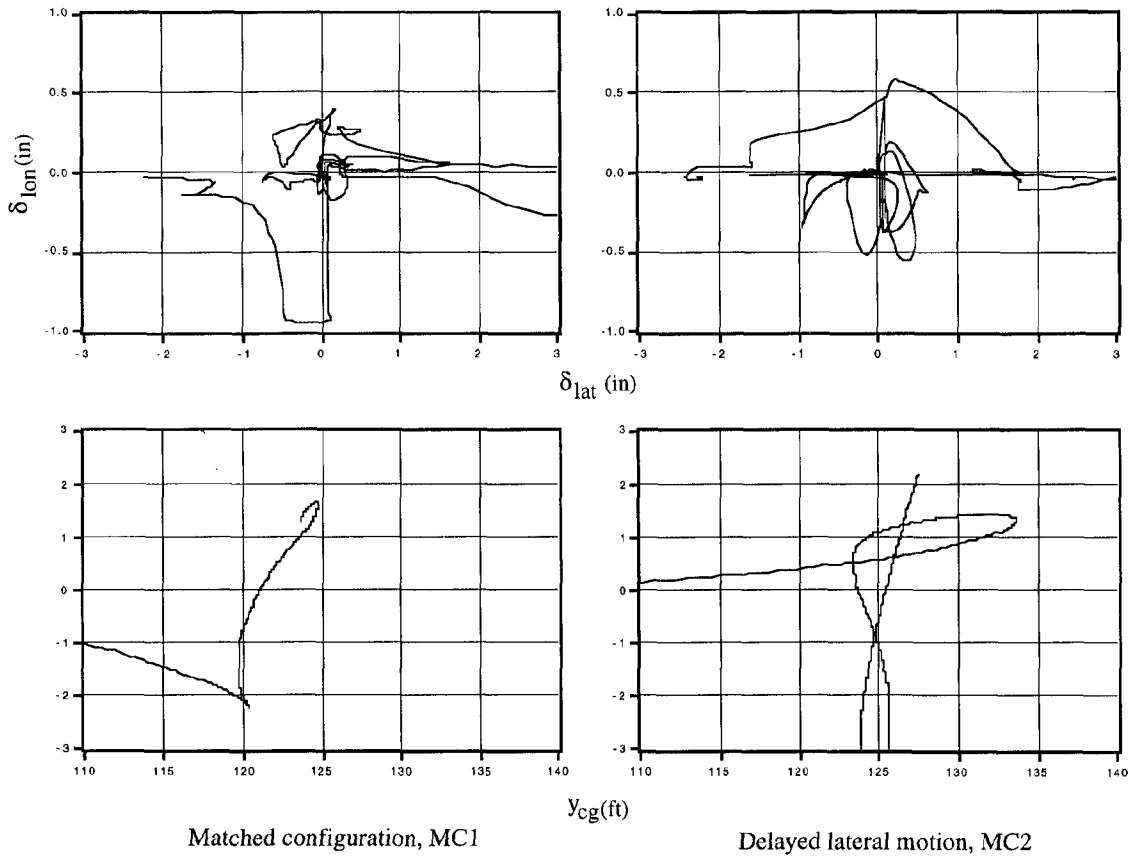


Figure 23. Pilot stick and hover position time traces for modified sidestep task

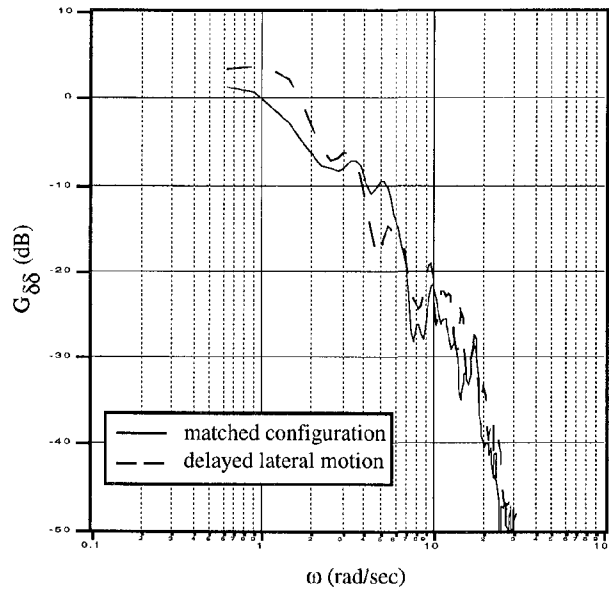


Figure 24. Pilot lateral control stick power spectral density response for modified sidestep task

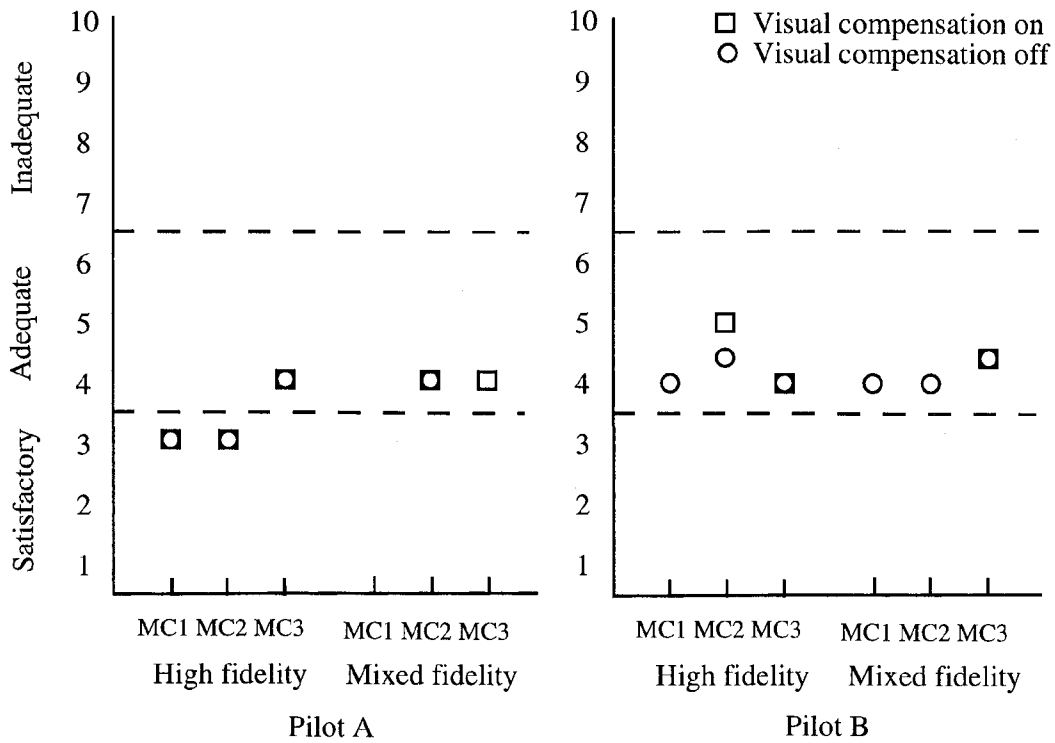


Figure 25. Pilot HQR with and without visual delay compensation